Available online at www.sciencedirect.com
ScienceDirect
Journal of Molecular Catalysis A: Chemical 270 (2007) 50–55
JOURNAL OF MOLECULAR CATALYSIS A: CHEMICAL
www.elsevier.com/locate/molcata

Synthesis, characterization and catalytic application of SBA-15 immobilized rare earth metal sandwiched polyoxometalates

Yan Zhou, Renlie Bao, Bin Yue *, Min Gu, Supeng Pei, Heyong He *

Department of Chemistry and Shanghai Key Laboratory of Molecular Catalysis and Innovative Materials, Fudan University, Shanghai 200433, PR China

Received 21 June 2006; received in revised form 19 January 2007; accepted 21 January 2007
Available online 24 January 2007

Abstract

Rare earth metal sandwiched Keggin-type heteropolyoxometalates, $K_{11}[RE(PW_{11}O_{39})_2]$ (RE–PW_{11}, RE = La, Ce, Pr, Nd, Sm, Eu, Dy and Y), were anchored onto aminosilylated mesoporous silica SBA-15 and the resulting RE–PW_{11}/APTS/SBA-15 materials were characterized by ICP, FT-IR, XRD, N_2 adsorption, ^{31}P MAS NMR and TEM. The RE–PW_{11} clusters preserve their structure in the surface-modified mesopores. The catalytic activity of RE–PW_{11} clusters was tested on heterogeneous oxidation of cyclohexene by H_2O_2. The interaction between RE–PW_{11} and amino groups grafted on the channel surface of SBA-15 leads to strong immobilization of RE–PW_{11} due to the introduction of the rare earth metal centre, which is against the leaching during the reaction.

Keywords: Rare earth metal sandwiched tungstophosphates; Aminosilylation; Mesoporous SBA-15; Oxidation; Cyclohexene

1. Introduction

The application of hydrogen peroxide in catalytic oxidation of organic compounds is of industrial importance. Hydrogen peroxide is an attractive oxidant, because it is inexpensive, environmentally clean, and easy to handle. Catalysts such as Ti-containing molecular sieves and polyoxometalates (POM) have been reported to exhibit high activity. In both heterogeneous and homogeneous systems, the oxidation of organic compounds with hydrogen peroxide catalyzed by POMs has been reported by many researchers [1–6]. Among the catalysts used, 12-phosphotungstic acid, $H_3PW_{12}O_{40}{\cdot}nH_2O$ is most extensively studied [7–15]. However, the application of POM catalysts still suffers from some drawbacks of the POM nature, particularly the low surface area (<5 $m^2\ g^{-1}$) leading to the low efficiency and the high solubility causing recycling difficulty and environmental problem.

The heterogenization of POM catalysts is an ideal way to solve the above problems. It is well accepted that by converting a homogeneous catalyst into a heterogeneous entity one may combine the activity and selectivity of the homogeneous catalyst with the ease of solid–liquid separation. Some promising heterogeneous POM systems such as insoluble polyoxotungstates [16,17], silica supported peroxotungstates [18,19], triphasic phosphotungstate [20] and phase transfer systems [21] have been reported recently. Previous studies of polyoxometalates supported on amorphous silica or mesoporous silica were mainly focused on the free acids of Keggin-type POMs supported on silica by the incipient wetness method [22–25]. For this preparation method the leaching of POM is rather significant. In some recent contributions, the anchoring of POM free-acids onto the amine groups modified silica surface aimed to minimize leaching of the cluster in washing or during the reaction cycle [6,18]. However, the leaching of polyoxometalate from the supports is still inevitable, which limits the application of these materials in catalysis.

Transition metal substituted POMs usually show high activity in the hydroxylation of phenols and their supported catalysts exhibit high resistance to leaching due to the strong interaction between the central transition metal ions and the surface of supports [2,6]. Rare earth metal sandwiched Keggin-type POM anions $[RE(PW_{11}O_{39})_2]^{n-}$ (RE = La, Ce, Pr, Nd, Sm, Eu, Dy and Y) normally also show catalytic activity in the homogeneous system [26,27]. However, the study of these catalysts in the heterogeneous system is hardly reported. In

* Corresponding authors. Tel.: +86 21 65642779; fax: +86 21 65642798.
E-mail addresses: yuebin@fudan.edu.cn (B. Yue), heyonghe@fudan.edu.cn (H. He).

1381-1169/$ – see front matter © 2007 Elsevier B.V. All rights reserved.
doi:10.1016/j.molcata.2007.01.034

the present work, the $[RE(PW_{11}O_{39})_2]^{n-}$ clusters have been anchored onto the aminosilylated surface of silica SBA-15 in order to minimize leaching. The obtained materials have been characterized by ICP, FT-IR, N_2 adsorption, TEM, XRD and ^{31}P MAS NMR. The results indicate that the POM clusters preserve their structure in the surface-modified mesopores. Their activity of cyclohexene oxidation using H_2O_2 as oxidant has been studied.

2. Experimental

2.1. Catalyst preparation

Rare earth metal nitrates and sulfates were prepared from their corresponding oxides (99.9%).

The preparation of $K_{11}[RE(PW_{11}O_{39})_2]\cdot nH_2O$ (RE = La, Ce, Pr, Nd, Sm, Eu, Dy and Y) followed the literature procedures with minor modifications [26,28]. 4.3 g dodecatungstophosphoric acid was dissolved in hot water. Concentrated rare earth metal(III) nitrate solution was added to a hot solution with a $H_3PW_{12}O_{40}$:$RE(NO_3)_3$ molar ratio of 2:1. Then, concentrated potassium acetate solution (10 g of potassium acetate in 10 ml of water at pH of 7 adjusted with acetic acid or nitric acid) was added dropwise under vigorous stirring. After potassium acetate solution was completely added, the mixture was kept without stirring for several minutes and filtered. When the filtrate was cooled to 5 °C, the desired salt was precipitated completely. The salt was recrystallized from water at least three times and dried in a desiccator over P_2O_5.

SBA-15 was synthesized using the block copolymer Pluronic P123 (Aldrich) and tetraethyl orthosilicate (TEOS, 98%, Aldrich) under acidic condition. After synthesis and removal of the template by calcination at 550 °C, the samples were dried at 180 °C for 3 h under vacuum. The aminosilylation was performed according to the literature method with minor modification. In a typical procedure, 1 g of SBA-15 was treated in a 30 ml refluxing toluene solution containing 1% γ-aminopropyltriethoxysilane (APTS) for 5 h [29,30]. The resulting material, APTS/SBA-15, was filtered, washed with toluene, and dried at 95 °C for 3 h to remove the remaining solvent.

The $K_{11}[RE(PW_{11}O_{39})_2]$ (denoted as RE–PW_{11}) are immobilized within the modified SBA-15 channels. A typical process is as follows: 2 g of APTS/SBA-15 was stirred in a 5 ml of aqueous solution containing 6.5×10^{-4} mol of RE–PW_{11} at 60 °C for 8 h. The resulting solid catalysts, RE–PW_{11}/APTS/SBA-15, were then filtered and washed with methanol three times to remove unanchored RE–PW_{11} and dried at 95 °C for 3 h. This simple two-step method is illustrated in Scheme 1.

RE–PW_{11} supported on unmodified SBA-15 are also synthesized through incipient wetness under similar conditions, the resulting materials were denoted by RE–PW_{11}/SBA-15.

2.2. Catalytic reaction

Catalytic tests were performed using 8 ml *tert*-butyl alcohol, 2.50 ml 30% (24 mmol) hydrogen peroxide, 0.838 g (10 mmol) cyclohexene, 0.150 g catalyst and 2 ml *n*-hexane as the internal

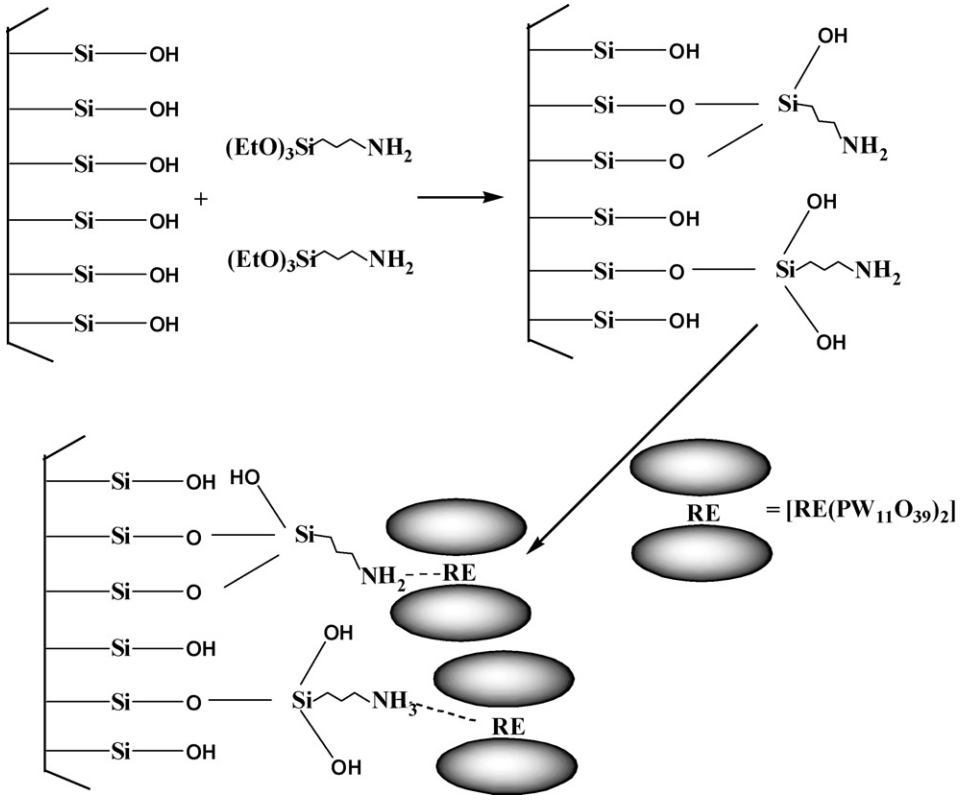

Scheme 1.

standard. The reactants were mixed in a round-bottom flask fitted with a reflux condenser and allowed to react at 60 °C for 4 h. After the reaction finished, aliquot was extracted and filtered. The products were analyzed with gas chromatography.

2.3. Characterization

Elemental analysis was carried out using a Thermo Elemental IRIS Intrepid ICP-AES. IR spectra were recorded on an AVATAR 360 Fourier transform infrared instrument at room temperature using KBr discs. The specific surface area, pore diameter and pore volume of the samples were determined from N_2 adsorption isotherms using a Micromeritics Tristar 3000 apparatus. ^{31}P MAS NMR spectra were recorded on a Bruker Avance DSX300 spectrometer. XRD patterns were recorded on a Bruker D8 advanced X-ray diffractometer using Cu Kα radiation with a voltage of 40 kV and a current of 40 mA. Identification of catalytic products was performed on a Finnigan Voyager GC–MS instrument. Samples were quantified on a GC-122 chromatograph with an Alltech EC-5 capillary column.

3. Results and discussion

3.1. Characterization of RE–PW_{11}/APTS/SBA-15

ICP elemental analysis was employed to testify the composition of RE–PW_{11} ligands supported onto the SBA-15 and the results are listed in Table 1. The PW_{11}:RE molar ratio close to 2:1 is consistent with that of bulk sandwiched RE–PW_{11}. The loads of RE–PW_{11} are in the range of *ca.* 30–34%. Similar RE–PW_{11} loadings indicate that they are similar in electrostatic interaction between different POM clusters and amine groups.

IR spectroscopy was used to determine the presence of the POM cluster on silica surfaces. Peak assignments are based on the literature values [31]. As shown in Fig. 1(a), the characteristic infrared fingerprints of pure Y–PW_{11} and Y–PW_{11}/APTS/SBA-15 in the region of *ca.* 700–1100 cm^{-1} are attributed to vibrations of P–O in the central PO_4 unit, and to W=O and W–O–W of PW_{11}, although bands at 900–1050 cm^{-1} are partially obscured by the presence of silica [27]. The results indicate that the primary POM structure remains intact after immobilization onto the mesoporous silica surface. This is also consistent with the ICP elemental analysis data (Table 1). Similar results

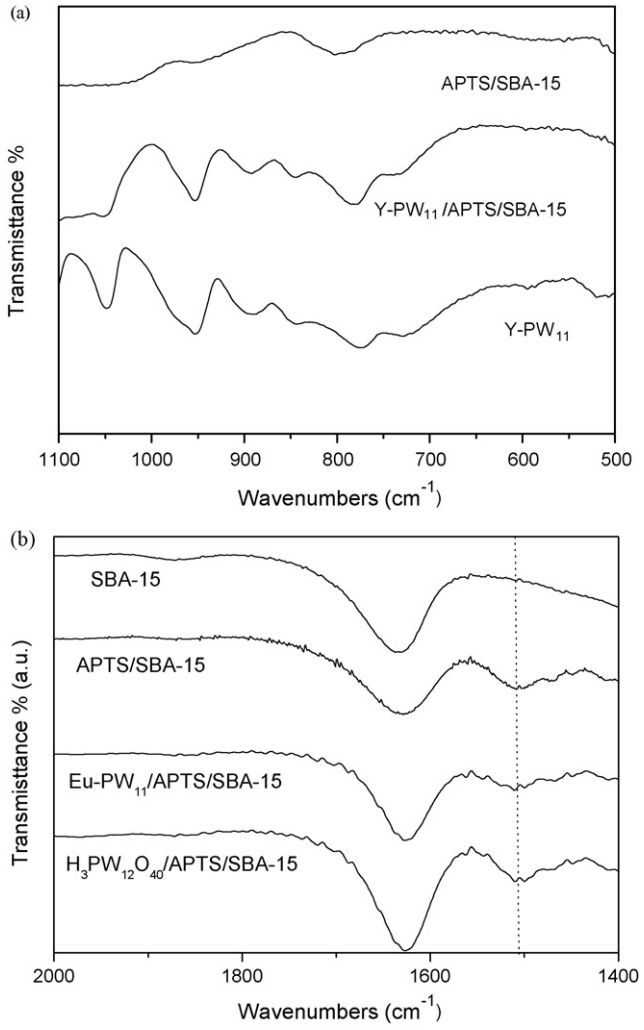

Fig. 1. IR spectra of (a) APTS/SBA-15, Y–PW_{11}/APTS/SBA-15 and bulk Y–PW_{11}, (b) SBA-15, APTS/SBA-15, Eu–PW_{11}/APTS/SBA-15 and $H_3PW_{12}O_{40}$/APTS/SBA-15.

(Table 2) were obtained in other RE–PW_{11}/APTS/SBA-15 spectra. Fig. 1(b) shows the IR spectra of SBA-15, APTS/SBA-15, Eu–PW_{11}/APTS/SBA-15 and $H_3PW_{12}O_{40}$/APTS/SBA-15. One may find that all three aminosilated samples exhibit the bands at 1508–1530 cm^{-1} attributed to vibrations of protonated amino groups, which indicates that part of the amino groups of RE–PW_{11}/APTS/SBA-15 are protonated.

Table 1
ICP elemental analysis of RE–PW_{11}/APTS/SBA-15

Sample	RE (wt%)	P (wt%)	W (wt%)	Si (wt%)	POM (wt%)
La–PW_{11}/APTS/SBA-15	0.725	0.337	22.6	23.2	30.6
Ce–PW_{11}/APTS/SBA-15	0.720	0.353	23.0	23.8	31.3
Pr–PW_{11}/APTS/SBA-15	0.767	0.337	23.0	23.8	31.3
Nd–PW_{11}/APTS/SBA-15	0.849	0.378	24.6	23.7	33.4
Sm–PW_{11}/APTS/SBA-15	0.823	0.339	22.1	23.3	30.1
Eu–PW_{11}/APTS/SBA-15	0.802	0.327	22.3	24.0	30.4
Dy–PW_{11}/APTS/SBA-15	0.747	0.307	22.6	23.9	30.8
Y–PW_{11}/APTS/SBA-15	0.459	0.386	24.4	23.9	32.8
PW_{12}/APTS/SBA-15	–	0.183	13.1	13.9	17.0

Table 2
The IR absorption bands of the samples

Sample	Adsorption bands (cm^{-1})					
	$\upsilon_{(P-O)}$		$\upsilon_{(W=O)}$		$\upsilon_{(W-O-W)}$	
$Y–PW_{11}$	1094	946	890	843	770	721
$fLa–PW_{11}$/APTS/SBA-15	1089	952	894	836	789	731
$Ce–PW_{11}$/APTS/SBA-15	1090	952	894	835	785	731
$Pr–PW_{11}$/APTS/SBA-15	1090	952	894	835	787	731
$Nd–PW_{11}$/APTS/SBA-15	1091	953	893	836	790	731
$Sm–PW_{11}$/APTS/SBA-15	1090	952	895	836	788	731
$Eu–PW_{11}$/APTS/SBA-15	1090	953	894	836	789	731
$Dy–PW_{11}$/APTS/SBA-15	1090	952	894	836	788	731
$Y–PW_{11}$/APTS/SBA-15	1094	953	888	841	777	731
PW_{12}/APTS/SBA-15	1089	952	891	832	783	731

Fig. 2 shows the low angle XRD patterns of APTS/SBA-15 and $Y–PW_{11}$/APTS/SBA-15 in the 2θ range of 0.5–5°. Both samples exhibit three peaks indexed to characteristic (1 0 0), (1 1 0) and (2 0 0) diffractions of hexagonal mesoporous SBA-15, which indicates that these samples consist of well-ordered channels [32]. Therefore, the primary structure of SBA-15 is maintained after aminosilylation and immobilization of $RE–PW_{11}$. The immobilization of $RE–PW_{11}$ inside SBA-15 channels results in a decrease in the intensity of all diffractions, which is probably attributed to the pore filling of the host material with $RE–PW_{11}$. Low angle XRD patterns of other $RE–PW_{11}$/APTS/SBA-15 give the same results.

The nitrogen sorption isotherm of $Y–PW_{11}$/APTS/SBA-15 in Fig. 3 is of type IV classification, which is a hysteresis loop typical of mesoporous materials [32]. The surface modified and $Y–PW_{11}$ immobilized samples retain the same shape of the isotherm as that of SBA-15. The physicochemical parameters of SBA-15 after immobilization of other $RE–PW_{11}$ are shown in Table 3. The results show that aminosilylation of the surface and immobilization of $RE–PW_{11}$ account for the decrease in pore volume and surface area. However, pore size of $RE–PW_{11}$/APTS/SBA-15 samples does not change significantly, which probably indicates that $RE–PW_{11}$ is only immobilized in part of the channels. The above characterization results confirm that $RE–PW_{11}$ clusters are located inside the channels and the mesoporous channels are still preserved.

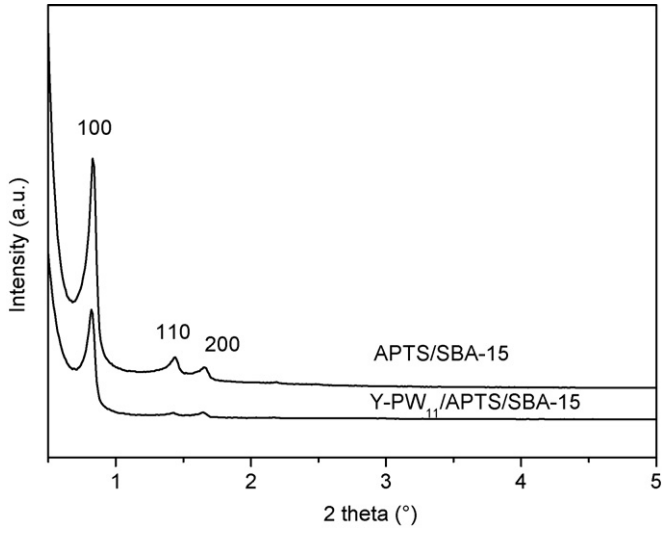

Fig. 2. Low-angle XRD patterns of APTS/SBA-15 and $Y–PW_{11}$/APTS/SBA-15.

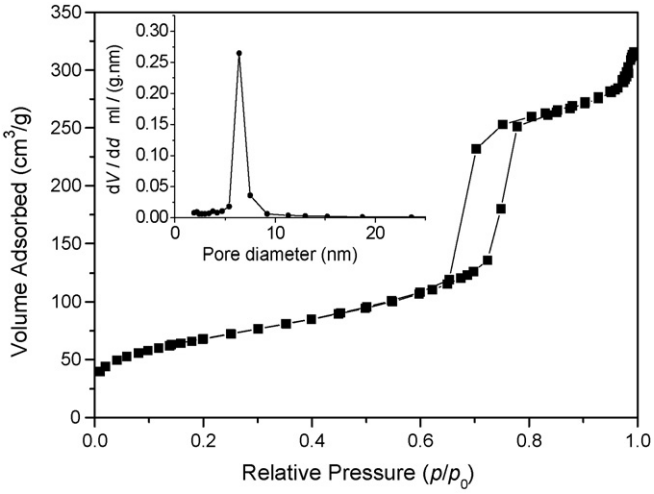

Fig. 3. N_2 adsorption–desorption isotherm of $Y–PW_{11}$/APTS/SBA-15. Insert: pore size distribution.

The ^{31}P NMR spectra of bulk $Y–PW_{11}$ and the immobilized $Y–PW_{11}$/APTS/SBA-15 (Fig. 4) show only one resonance at −12.9 and −13.0 ppm with full-width-at-half-maximum (FWHM) of 336 and 200 Hz, respectively. The similar chemical shifts indicate that the PW_{11} and the sandwiched structure are generally unchanged after immobilization. The slight shift is possibly caused by slight change of local structural environment of P in the isolated POM anion after introduced in SBA-15 compared to the POM in bulk crystal. It is interesting to note the considerable decrease in FWHM after introducing $Y–PW_{11}$ onto the channel surface of the support. Since there is only one P site in the POM anion attributed to the NMR resonance, the decrease in FWHM is possibly caused by easier motion of isolated POM anion after introduced in SBA-15.

In Fig. 5, the exemplified TEM images of the $Sm–PW_{11}$/APTS/SBA-15 further demonstrate that the hexagonal ordered channel structure of SBA-15 has no significant change after aminosilylation of SBA-15 and immobilization of $Sm–PW_{11}$ into the channels. The polyoxometalates filled in the pores of

Table 3
Physicochemical properties of SBA-15 and its modified samples

Sample	Surface area ($m^2\ g^{-1}$)	Pore diameter (nm)	Pore volume ($cm^3\ g^{-1}$)
SBA-15	674	7.78	1.25
APTS/SBA-15	334	6.72	0.639
$La–PW_{11}$/APTS/SBA-15	308	6.24	0.496
$Ce–PW_{11}$/APTS/SBA-15	278	7.59	0.465
$Pr–PW_{11}$/APTS/SBA-15	270	7.56	0.456
$Nd–PW_{11}$/APTS/SBA-15	277	7.46	0.463
$Sm–PW_{11}$/APTS/SBA-15	272	7.32	0.454
$Eu–PW_{11}$/APTS/SBA-15	278	7.25	0.459
$Dy–PW_{11}$/APTS/SBA-15	278	7.32	0.471
$Y–PW_{11}$/APTS/SBA-15	302	7.32	0.458

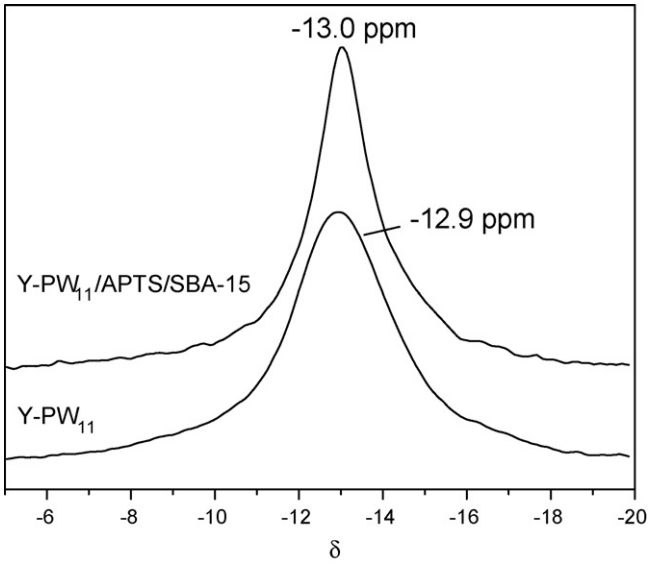

Fig. 4. ^{31}P MAS NMR spectra of Y–PW_{11}/APTS/SBA-15 and bulk Y–PW_{11}.

SBA-15 are shown by the highly contrast lines in comparison with pure SBA-15.

3.2. Catalytic testing

The catalytic activity of RE–PW_{11}/APTS/SBA-15 in heterogeneous oxidation of cyclohexene with hydrogen peroxide was tested and the results are shown in Table 4. Besides cyclohexene epoxide as the main product, a variety of byproducts such as cyclohexanone, 2-cyclohexen-1-ol, 2-cyclohexen-1-one and *trans*-1,2-cyclohexanediol are observed, indicating that the reaction was complicated.

The results indicate that cerium and heavier lanthanide complexes are generally somehow less effective for oxidation of cyclohexene (Table 4). Considering its redox potential, Ce(III) may be partially oxidized by H_2O_2 to Ce(IV), leading to the decrease in the amount of active species. For the heavier lanthanides there is a lanthanide contraction effect, resulting in stronger ionic interaction between the smaller central lanthanum atom and the two PW_{11} moieties. This makes the rendering degradation by H_2O_2 to polyperoxotungstates more difficult, lowering the catalytic activity [26,27].

Table 4
The catalytic performance of RE–PW_{11}/APTS/SBA-15[a]

Catalyst	Conversion of cyclohexene (%)	Yield of cyclohexene epoxide (%)
La–PW_{11}/APTS/SBA-15	67 (81)[b]	49 (77)[b]
Ce–PW_{11}/APTS/SBA-15	44 (67)[b]	30 (51)[b]
Pr–PW_{11}/APTS/SBA-15	57 (76)[b]	46 (64)[b]
Nd–PW_{11}/APTS/SBA-15	56 (76)[b]	45 (63)[b]
Sm–PW_{11}/APTS/SBA-15	55 (73)[b]	46 (61)[b]
Eu–PW_{11}/APTS/SBA-15	54 (74)[b]	46 (63)[b]
Dy–PW_{11}/APTS/SBA-15	53 (72)[b]	45 (61)[b]
Y–PW_{11}/APTS/SBA-15	81 (89)[b]	64 (61)[b]
Y–PW_{11}/APTS/SBA-15[c]	79	62
PW_{12}/APTS/SBA-15	99	69
PW_{12}/APTS/SBA-15[c]	67	53
Nd–PW_{11}/SBA-15	57	47
Nd–PW_{11}/SBA-15[c]	–	–
Sm–PW_{11}/SBA-15	56	47
Sm–PW_{11}/SBA-15[c]	–	–

[a] Reaction conditions: 8 ml *t*-butanol, 2.5 ml 30% (24 mmol) hydrogen peroxide, 0.838 g (10 mmol) cyclohexene, 0.150 g RE–PW_{11}/APTS/SBA-15 (or RE–PW_{11}) and 2 ml *n*-hexane (internal standard), 60 °C, 4 h.
[b] Catalytic performance of bulk RE–PW_{11} (in parentheses).
[c] Catalyst recycled after the fifth run.

It is also shown in Table 4 that the absolute conversion for bulk RE–PW_{11} are higher than those for the immobilized ones, but the latter have much higher catalytic efficiency per POM unit than the bulk POM. This higher efficiency should be attributed to the high dispersion of POM. When bulk RE–PW_{11} is used as catalyst, the dissolution of bulk RE–PW_{11} is significant after 4 h reaction. Nearly half amount of bulk RE–PW_{11} leaches into the solutions after solid–liquid separation. However, RE–PW_{11}/APTS/SBA-15 shows high stability in polar solvent, where the leaching of POM is negligible and the catalytic activity of the five times recycled catalyst remains unchanged, indicating that the strong interaction between RE–PW_{11} and the amino groups on the silica surface prevents leaching of active species of POM.

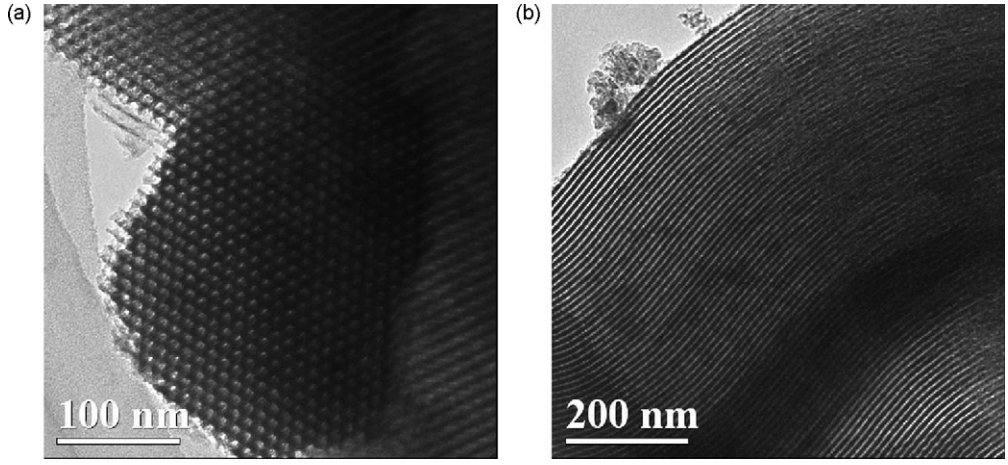

Fig. 5. TEM images of Sm–PW_{11}/APTS/SBA-15 parallel (a) and perpendicular (b) to the channel direction of SBA-15.

According to the ^{31}P NMR study, no signal is detected in the solution after reaction for 12 h with the Y–PW_{11}/APTS/SBA-15 catalyst, showing that the loss of Y–PW_{11} could be neglected. In contrast, under the same reaction condition the conversion of cyclohexene decreases significantly over PW_{12}/APTS/SBA-15, and ^{31}P NMR signal could be detected in the filtered reaction solution. Therefore, the introduction of rare earth centre into POM helps enhance the interaction between RE–PW_{11} and the amino groups grafted on the silica channel surface. The enhanced interaction prevents POMs from leaching into the reaction solution, although the mechanism how the RE centre works is not clear yet.

The catalytic activity and reusability of RE–PW_{11} (Sm–PW_{11} and Nd–PW_{11} were chosen) supported on unmodified SBA-15 were also tested. The amount of RE–PW_{11} and other reaction conditions are the same as those for RE–PW_{11}/APTS/SBA-15. In the first run, the cyclohexene conversion and cyclohexene epoxide yield over RE–PW_{11}/SBA-15 are similar to those over RE–PW_{11}/APTS/SBA-15. However, the leaching of POM from RE–PW_{11}/SBA-15 is significant. RE–PW_{11}/SBA-15 recycled after the fifth run shows almost no catalytic activity, and none of RE, P, W can be detected by the ICP elemental analysis. Thus, it could be concluded that the amino group on SBA-15 has the effect of immobilizing RE–PW_{11}.

To check whether the Y–PW_{11} immobilized on APTS/SBA-15 support or the dissolved homogeneous Y–PW_{11} is the real catalyst responsible for the present oxidation, the following experiment was carried out [33]. After reaction for 2 h in which the cyclohexene conversion reached *ca*. 41%, the reaction mixture was filtered and then the mother liquor (filtrate) was allowed to react for another 8 h under the same reaction condition. No significant activity was observed, demonstrating that the active species are not the dissolved Y–PW_{11} leached from Y–PW_{11}/APTS/SBA-15. Therefore, it is reasonable to suggest that the present catalysis is heterogeneous in nature.

4. Conclusion

The rare earth metal sandwiched POM, RE–PW_{11}, is immobilized in the channels of aminosilylated ATPS/SBA-15. RE–PW_{11}/APTS/SBA-15 combines catalytic activity of RE–PW_{11} and high surface area of SBA-15 and shows higher catalytic efficiency per POM unit than the bulk POM. There is strong interaction between RE–PW_{11} and amino groups grafted on the silica channel surface, leading to negligible leaching of RE–PW_{11} species and ease in separation in solid–liquid phase after catalytic reaction. Such a kind of material may be used as environmentally benign heterogeneous catalyst for the oxidation of olefins under mild conditions.

Acknowledgements

This work was supported by the National Basic Research Program of China (2003CB615807), the National Natural Science Foundation of China (Grant Nos. 20421303, 20633030, 20371013) and Shanghai Science and Technology Committee (05DZ22313, 06DJ14006).

References

[1] T. Okuhara, N. Mizuno, M. Misono, Appl. Catal. A: Gen. 222 (2001) 63.
[2] C.L. Hill, C.M. Prosser-McCartha, Coord. Chem. Rev. 143 (1995) 407.
[3] N. Mizuno, M. Misono, Chem. Rev. 98 (1998) 199.
[4] I.V. Kozhevnikov, Chem. Rev. 98 (1998) 171.
[5] A. Corma, Chem. Rev. 95 (1995) 559.
[6] B.J.S. Johnson, A. Stein, Inorg. Chem. 40 (2001) 801.
[7] D.P. Das, K.M. Parida, Appl. Catal. A: Gen. 305 (2006) 32.
[8] K. Nowińska, R. Fórmaniak, W. Kaleta, A. Wacław, Appl. Catal. A: Gen. 256 (2003) 115.
[9] F.M. Collins, A.R. Lucy, C. Sharp, J. Mol. Catal. A: Chem. 117 (1997) 397.
[10] M. Te, C. Fairbridge, Z. Ring, Appl. Catal. A: Gen. 219 (2001) 267.
[11] C. Aubry, G. Chottard, N. Platzer, J.-M. Brégeault, R. Thouvenot, F. Chauveau, C. Huet, H. Ledon, Inorg. Chem. 30 (1991) 4409.
[12] Y. Ding, Q. Gao, G.X. Li, H.P. Zhang, J.M. Wang, L. Yan, J.S. Suo, J. Mol. Catal. A: Chem. 218 (2004) 161.
[13] A. Ghanbari-Siahkali, A. Philippou, J. Dwyer, M.W. Anderson, Appl. Catal. A: Gen. 192 (2000) 57.
[14] M.J. Verhoef, P.J. Kooxman, J.A. Peters, H. van Bekkum, Micropor. Mesopor. Mater. 27 (1999) 365.
[15] I.V. Kozhevnikov, A. Sinnema, R.J.J. Jansen, K. Pamin, H. van Bekkum, Catal. Lett. 30 (1995) 241.
[16] K. Kamata, K. Yonehara, Y. Sumida, K. Yamaguchi, S. Hikichi, N. Mizuno, Science 300 (2003) 964.
[17] M.V. Vasylyev, R. Neumann, J. Am. Chem. Soc. 126 (2004) 884.
[18] J.-M. Brégeault, M. Vennat, L. Salles, J.-Y. Piquemal, Y. Mahha, E. Briot, P.C. Bakala, A. Atlamsani, R. Thouvenot, J. Mol. Catal. A: Chem. 250 (2006) 177.
[19] K. Yamaguchi, C. Yoshida, S. Uchida, N. Mizuno, J. Am. Chem. Soc. 127 (2005) 530.
[20] Y.M.A. Yamada, M. Ichinohe, H. Takahashi, S. Ikegami, Org. Lett. 3 (2001) 1837.
[21] Z.W. Xi, N. Zhou, Y. Sun, K.L. Li, Science 292 (2001) 1139.
[22] G.D. Yadav, H.G. Manyar, Micropor. Mesopor. Mater. 63 (2003) 85.
[23] I.V. Kozhevnikov, K.R. Kloestra, A. Sinnema, H.W. Zandbergen, H. van Bekkum, J. Mol. Catal. A: Chem. 114 (1996) 287.
[24] T. Blasco, A. Corma, A. Martínez, P. Martínez-Escolano, J. Catal. 177 (1998) 306.
[25] F. Marme, G. Coudurier, J.C. Védrine, Micropor. Mesopor. Mater. 22 (1998) 151.
[26] W.P. Griffith, R.G.H. Moreea, H.I.S. Nogueira, Polyhedron 15 (1996) 3493.
[27] W.P. Griffith, N. Morley-Smith, H.I.S. Nogueira, A.G.F. Shoair, M. Suriaatmaja, A.J.P. White, D.J. Williams, J. Organomet. Chem. 607 (2000) 146.
[28] N. Haraguchi, Y. Okaue, T. Isobe, Y. Matsuda, Inorg. Chem. 33 (1994) 1015.
[29] K.K. Zhu, B. Yue, W.Z. Zhou, H.Y. He, Chem. Commun. (2003) 98.
[30] B. Yue, D.J. Tan, S.R. Yan, Y. Zhou, K.K. Zhu, J.F. Pan, J.H. Zhuang, H.Y. He, Chin. J. Chem. 23 (2005) 32.
[31] S. Choi, Y. Wang, Z.M. Nie, J. Liu, C.H.F. Peden, Catal. Today 55 (2000) 117.
[32] D.Y. Zhao, J.L. Feng, Q.S. Huo, N. Melosh, G.H. Fredrickson, B.F. Chmelka, G.D. Stucky, Science 279 (1998) 548.
[33] R.A. Sheldon, M. Wallau, I.W.C.E. Arends, U. Schuchardt, Acc. Chem. Res. 31 (1998) 8.